doi:10.1017/S1431927615013239

A Novel Monochromator with Double Cylindrical Lenses

Takashi Ogawa, Boklae Cho, Sang Jung Ahn

Center for Advanced Instrumentation, Division of Industrial Metrology, Korea Research Institute of Standards and Science, Daejeon, Republic of Korea

Recently, various types of monochromators (MCs) have been proposed for advanced instruments such as the (scanning) transmission electron microscope ((S)TEM) [1,2], the scanning electron microscope (SEM) [3], and microscopes that utilize electron energy loss spectroscopy (EELS). There are several advantages with regard to the use of MCs. First, these devices offer improvements in the spatial resolution in low-energy regimes by reducing the contribution of chromatic aberrations. Second, they offer improvements in the energy resolution of the EELS spectra. Further improvements are necessary to reveal new information about specimens, such as the phonon signals. In addition, industry applications require simple and robust structures for MCs. In this study, we propose a novel MC with a high energy resolution and a simple structure. It consists of two electrostatic cylindrical lenses (CLs) in highly excited retarding mode, similar to a Möllenstedt energy analyzer [4]. They are placed in mid-plane symmetry and both are shifted from the optical axis of a microscope. A detailed discussion of the MC is given below.

For this MC, an offset CL is a key component. We give an outline of its physical behavior. A CL consists of three electrodes, similar to an Einzel lens but with rectangular openings in the center. This offers a stronger focusing effect in the X direction of the shorter side of the openings and a weaker focus in the Y direction. The electrons travel in the Z direction. The electrostatic potential of a CL can be expressed as follows:

$$\Phi(x,y,z) \cong \phi(z) - \phi''(z)x^2/4 + \cdots . \quad (1)$$

Ohiwa introduced the idea of a moving objective lens (MOL), which shows that superposition of a deflection field on a lens field is equivalent to displacement of the lens [5]. If the displacement of a CL is X_d, the potential of the offset CL is given by

$$\Phi(x - X_d, y, z) \cong \Phi(x,y,z) - X_d \frac{\partial \Phi}{\partial x} + \cdots \cong \phi(z) - \frac{\phi''(z)x^2}{4} + X_d \frac{\phi''(z)x}{2} + \cdots . \quad (2)$$

The third term corresponds to the deflection effect caused by the displacement X_d. The deflection function can be expressed as

$$F_{1x}(z) = X_d \phi''(z)/2 . \quad (3)$$

Smith and Munro derived a unified aberration theory for electrostatic lenses and multipoles [6]. We apply their theory to offset CLs. The paraxial ray equation can be written as follows:

$$x'' + \phi' x'/2\phi + \phi'' x/4\phi = F_{1x}/2\phi . \quad (4)$$

Two independent, homogeneous solutions of Eq. 3 can be written as an axial ray x_a and a field ray x_b. The inhomogeneous form of Eq. 3 can be solved by the variation of parameters method. The solution x_c can be written as

$$x_c(z) = \frac{x_a(z)}{\sqrt{\phi(z_0)}} \int_{z_o}^{z} \frac{F_{1x}(\zeta)\, x_b(\zeta)}{2\sqrt{\phi(\zeta)}} d\zeta - \frac{x_b(z)}{\sqrt{\phi(z_0)}} \int_{z_o}^{z} \frac{F_{1x}(\zeta)\, x_a(\zeta)}{2\sqrt{\phi(\zeta)}} d\zeta . \quad (5)$$

Eq. 5 shows that defection function F_{1x} produces deflection ray x_c. The energy deviation, $\Delta\phi$, causes displacement δx_c to the original position of the trajectories. Here, δx_c includes not only the axial and transverse chromatic aberrations of the CL but also the displacement x_κ for deflection ray x_c, which takes

$$x_\kappa = C\, \Delta\phi\, x_c(z_i)/\phi(z_i), \text{ where } C = \left[\frac{\sqrt{\phi}}{x'_a x_c}\right]_{z_i} \int_{z_o}^{z_i} \frac{x_a x_c''}{\sqrt{\phi}} dz . \quad (6)$$

If we adopt this deflection ray x_c as an optical axis, the displacement x_κ can be considered as the energy dispersion to the optical axis by the energy deviation $\Delta\phi$. The common expression of energy dispersion is $D_\kappa = x_\kappa/\Delta\phi$. This discussion shows that the offset CL has an additional deflection effect and that this causes the energy dispersion. This enables the adoption of the offset CLs as deflection units for the MC.
Next, we analyze the MC in detail by direct ray trace methods. We use EO-3D software by MEBS Ltd. to calculate the trajectories in three dimensions. The detailed dimensions of the CLs are as follows: the thickness of the electrodes is 10 mm, the gap between the electrodes is 10 mm, the shorter side of the opening is 10 mm, and the longer side of the opening is 100 mm. Figure 1 shows the schematics of the MC and the rays. The figure shows two cylindrical lenses (CL_1, CL_2), two round transfer lenses (TL_1, TL_2), two apertures, and an electron emitter. All the CLs and the TLs are arranged in mid-plane symmetry with Z_2. The two CLs are equally excited, with the same focal length of f_c. The centers of CL_1 and CL_2 are separated by $2f_c$. Both of the CLs are offset by X_d from the optical axis of a microscope in the X direction, corresponding to the shorter side of the rectangular openings of the CLs. The two values f_c and X_d are related to the excitations of the CLs. Later discussions adopt f_c = 40 mm and X_d = 0.407 mm, where the center electrode voltages of the CLs (V_{CL}) are -0.248 kV from the emitter. The MC has two apertures. One is the entrance aperture, which is located in the front focal plane of CL_1 (Z_1) to limit the incident angles of the emitted electrons. The other is the energy selection aperture, which is located at Z_2 to select the energy-dispersed rays. On the front side, the electron emitter is placed at Z_0. TL_1 and TL_2 are arranged along the optical axis of the microscope to achieve stigmatic and dispersion-free imaging of the emitter at the exit plane (Z_4) of the MC. TL_1, whose focal length is f_1, is located at Z_0+f_1 to collimate the incident rays from the emitter. TL_2 with a focal length of f_2 is placed at Z_3+f_2 to focus the rays on Z_4. The lens effects of the two TLs are identical in the X and Y directions.

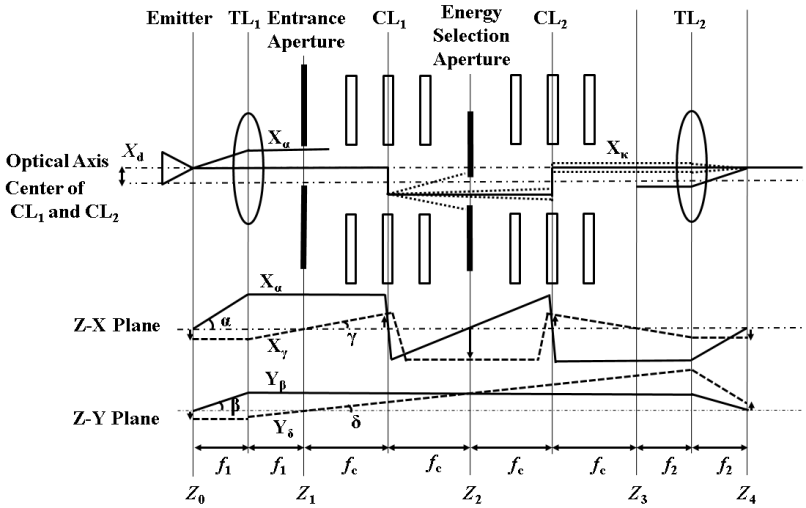

Figure 1. Schematics of the MC and the rays. The definitions of the planes (Z_0-Z_4) and focal lengths (f_c, f_1, f_2) are given.

The total optics of the MC becomes symmetric with the middle plane Z_2. In the region of Z_0-Z_1, the rays are identical in the X and Y directions. However, the optical paths in the two directions differ in the region of Z_1-Z_3 because the CLs have astigmatic focusing effects. Figure 2 shows the results of ray trace simulations in this region. The primary energy E_0 of the electron beams is 4 keV. Figure 2a shows the optical axis in the X direction. The axis, which is offset by X_d to the center axis of the CLs, is deflected steeply at the center of CL_1 and becomes parallel at Z_2. By succeeding CL_2, the axis is deflected back to the original axis at Z_3. The optical axis satisfies the condition of mid-plane symmetry with Z_2.

https://doi.org/10.1017/S1431927615013239 Published online by Cambridge University Press

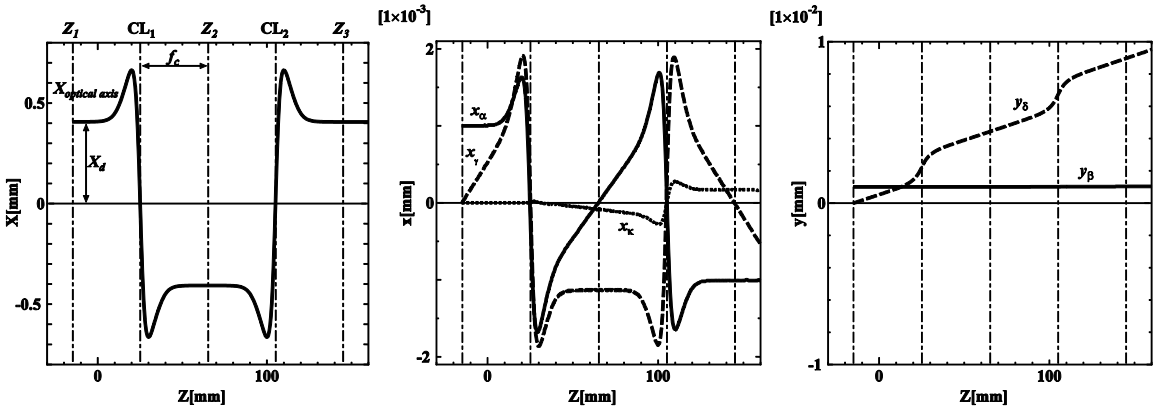

(a) (b) (c)

Figure 2. Simulated trajectories in the region of Z_1-Z_3, which is a part of the MC. (a) Optical axis. (b) X fundamental rays and an energy dispersive ray. (c) Y fundamental rays.

Figure 2b shows the fundamental rays (X_α, X_γ) and the energy dispersive ray (X_κ) in the X direction. The initial conditions are as follows: the offset distance of X_α is 1.0 μm, the inclined angle of X_γ is 3.5e^{-5} rad, and the energy deviation of X_κ is 1.0e^{-6}. The X_α ray has three intermediate image planes and shows asymmetry with Z_2. The X_γ ray has four image planes and shows symmetry with Z_2. In the X direction, an object in Z_1 is transferred to an image in Z_3 at a magnification of -1 by the CLs. The dispersive ray X_κ shows energy dispersion D_κ of 23 μm/eV at Z_2. The X_κ ray becomes parallel to the optical axis and the X_α ray at Z_3, which means that the angular energy dispersion $(a|\kappa)$ vanishes there. The mathematic expression of $(a|\kappa)$ is based on the textbook [7]. Figure 2c shows the fundamental rays (Y_β, Y_δ) in the Y direction. The initial conditions are identical to those in the X directions. Because the CLs have weak focusing power in the Y direction, the two rays have no intermediate image plane. The Y_β ray remains straight and the Y_δ ray is slightly shifted twice to the off-axis direction at each center of the CLs without changing the angle. After passing the CLs, TL_2 focuses the X_α and Y_β rays stigmatically on the exiting plane Z_4, as shown in Figure 1. Also, TL_2 focuses the X_κ ray, which means that the lateral energy dispersion $(x|\kappa)$ vanishes at the exit of the MC. In total, the MC realizes optics with stigmatic and lateral dispersion-free imaging. Moreover, the emitter is imaged with a magnification of |1| if the excitations of TL_1 and TL_2 are identical. The values of f_1 and f_2 are 10 mm, as discussed below.

Next, we evaluate the performance of the MC. Figure 3 presents the aberration figures and Table 1 summarizes the characteristics of the MC. Figure 3 shows the beam distributions in the incident currents I_{in} of 100, 300, and 1000 pA at the middle plane Z_2 (upper figures) and at the exiting plane Z_4 (lower figures). In addition, different colors represent the energy conditions of E_0, $E_0+\delta_\kappa/2$, and $E_0-\delta_\kappa/2$, and each value of δ_κ is summarized in Table 1. The other simulation conditions are as follows: Primary energy E_0: 4 keV, excitation voltages of CLs V_{CL}: -0.248 kV, number of trajectories: 3000, emitter type: Schottky emitter, virtual source diameter: 28 nm, angular current density: 500 μA/sr, energy spread in FWHM: 0.833 eV [8]. The aberration figures are constituted from a large number of trajectories whose initial conditions are randomly generated given the above simulation conditions. The energy selection slit widths d_s are calculated from the beam distributions at Z_2. The energy resolutions δ_κ are calculated by the equation $\delta_\kappa = 2d_s/D_\kappa$. The exiting currents I_{out} are calculated from the ratio of the electrons included in the energy range of δ_κ by postulating the energy distribution as a Gaussian with the energy spread described above.

https://doi.org/10.1017/S1431927615013239 Published online by Cambridge University Press

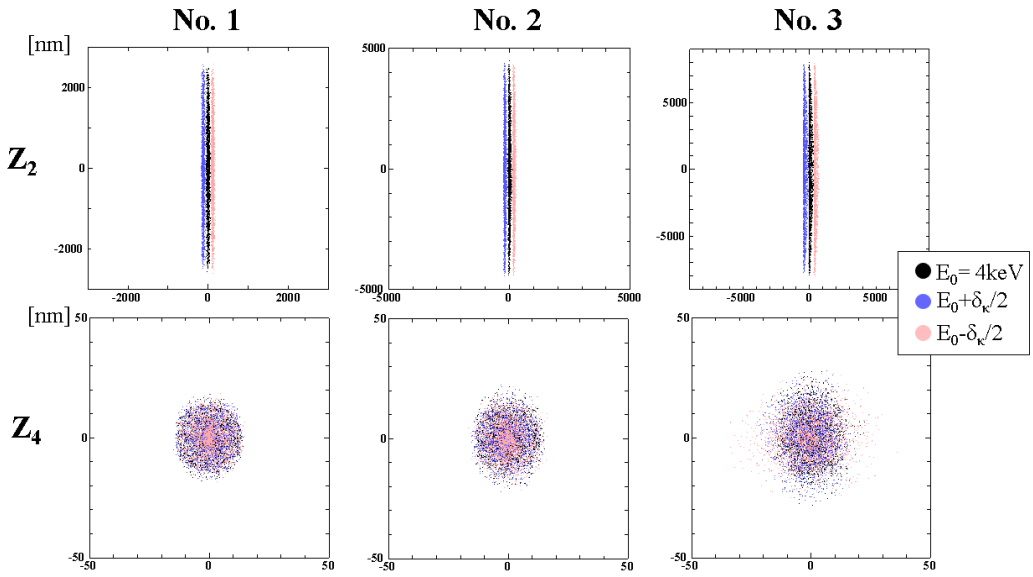

Figure 3. Aberration figures in the three incident currents conditions on the Z_2 and Z_4 planes.

Condition	Incident current I_{in} (pA)	Exit current I_{out} (pA)	Slit width d_s (nm)	Energy resolution δ_κ (meV)
No. 1	100	1.7	110	9.4
No. 2	300	7.1	180	15.4
No. 3	1000	50.4	390	33.5

Table 1. The characteristics of the MC as calculated with Figure 3.

The upper figures in Figure 3 clearly show that the rays are line-focused and energy dispersive at the middle plane Z_2. By inserting slit-shaped apertures, an energy-selecting function is realized. Furthermore, the lower figures in Figure 3 show that the rays are focused stigmatically at the exit plane Z_4 due to their symmetry. Also, the different rays in terms of energy, as shown in different colors, are focused on the same position. This indicates that they are lateral dispersion-free, $(x|\kappa)$ =0, at the exit plane Z_4. These results confirm that this optics can serve as a MC. In the smallest current condition of No. 1, the beam diameter is about 30 nm at Z_4. Considering that the virtual source diameter is 28 nm, this optics images the emitter with unit magnification at the exit. The energy resolution is better than 10 meV. By increasing the beam current, the beam shapes begin to blur. The beam profiles at Z_2 become asymmetric in the X direction and more triangular due to second-order aberrations. In contrast, the beam profiles at Z_4 show broad beam tails, but they remain symmetric in the X direction. These results imply that second-order aberrations are canceled and third-order aberrations are dominant on the exit plane Z_4. This is due to mid-plane symmetry of the optics. In the condition of No. 3, the energy resolution is approximately 34 meV. These results imply the potential of this optics as a high-performance MC.

We discuss the advantages and disadvantages of the MC with CLs by comparing it to other MCs. This MC is lateral dispersion-free, $(x|\kappa)$ =0, at the exit plane Z_4, as shown in Figure 3. Therefore, this MC is better than single-stage MCs [2,3,9]. It can prevent rainbow illumination, which can cause limitations in

https://doi.org/10.1017/S1431927615013239 Published online by Cambridge University Press

the TEM operation conditions. However, the angular energy dispersion $(a|\kappa)$ of the MC remains at Z_4. This means that the energy dispersive ray X_κ is inclined toward the optical axis at Z_4, as shown in Figure 1. With regard to this point, the MC is inferior to an electrostatic Ω-shaped MC [1] and a magnetic α-shaped MC [10], where both $(x|\kappa)$ and $(a|\kappa)$ are canceled. This MC can be classified into the same category as MCs with multiple Wien filters [11-13], where $(x|\kappa) = 0$ and $(a|\kappa) \neq 0$. From a different point of view, second-order aberrations of the MC are canceled at Z_4 but not at the middle plane Z_2, as shown in Figure 3. The aberrations at Z_2 can deteriorate the energy resolution and cause non-isochromatic energy selection [14]. The Ω-MC corrects the aberrations by curvatures of toroidal electrodes. The α-MC corrects them by hexapoles located in the front and back of the main prism. The multiple Wien-filter MCs cancel the aberrations at the exit, but not on the middle energy-selecting plane. With regard to the corrected ranks of aberrations, a MC with CLs can be classified into the same category as MCs with multiple Wien filters [11-13]. This is worse than sophisticated MCs [1,10] but better than single-stage MCs [2,3,9]. With the loss of its simplicity, this MC can be improved further by canceling aberrations with additional correctors. To cancel $(x|\kappa)$ and $(a|\kappa)$ at Z_4, the X_κ ray should be parallel to the optical axis at the middle plane Z_2. This condition can be achieved by placing two quadrupoles at the regions of CL_1-Z_2 and Z_2-CL_2, similar to the α-MC [10]. Canceling the second-order aberrations on the middle plane Z_2 can be achieved by placing two hexapoles at the regions of Z_1-CL_1 and CL_2-Z_1, similar to sector magnets [7,10,14].

This MC has asymmetric internal optical paths, where the rays have three crossovers in the X direction but no crossover in the Y direction. This can avoid additional beam blur due to electron-electron interactions caused by stigmatic images with a high current density, similar to the Ω-MC [1]. However, asymmetry of the beam profile at the middle plane Z_2 is greater than that of the Ω-MC due to its weak focusing power in the Y direction. This may impose some difficulties in the manufacturing of the energy selection aperture due to the high aspect ratio. Imperfections in the aperture may cause an inhomogeneous current distribution in the X and Y directions of the exiting beams. The aperture can be fabricated using the latest nano-processing techniques, such as EB lithography or a focused ion beam. From a different standpoint, this MC utilizes CLs in retarding mode. At the centers of the CLs, low-energy electrons are expected to be weak against disturbances such as external magnetic fields. This is also a disadvantage of the MC. For a practical design, double magnetic shields with high permeability, made of permalloy, should be implemented outside of the CLs. These are often adopted in low-energy electron analyzers.

It should be noted that a significant advantage of the MC is its simple optical configuration without multipole optics. Through the use of CLs as deflection elements, the mechanical structures, electronics, and control units can be simplified compared to other MCs with complicated optics. The Ω-MC adopts four deflection units with eight toroidal electrodes, which have different curvatures in not only the horizontal but also the vertical sections. The curvatures are determined by a simulation to achieve focusing power in the Y direction and the compensation of second-order aberrations. To manufacture the electrodes, sophisticated machining techniques for 3D curved surfaces are necessary. Also, a high level of alignments of the electrodes in 3D is required. MCs with Wien filters adopt multipole units in several stages, which also require fine machining and the alignment of separate poles to achieve the expected performance level. The α-MC adopts three main deflectors, 14 quadrupoles, and eight hexapoles. To control these units, a large number of power sources, which should be stable and low levels of noise, are necessary. Compared to these MCs, the MC with the CLs has a simple configuration. For CLs, rectangle openings in flat plate electrodes are necessary. Although they require accurate

https://doi.org/10.1017/S1431927615013239 Published online by Cambridge University Press

machining, this can be realized by conventional machining tools. The MC has an advantage in its assembly process because CLs consist of flat plate electrodes without separations in the azimuth directions. In addition, the MC requires only two electronic units for two CLs. The number of units is low compared to other MCs. This brings a benefit when the MC is used for the HV regions of electron guns. Two additional units are necessary for TLs, but they can be used as the condenser lenses of microscopes. These reductions of complexity are a great advantage for MCs. They lead to a highly stable, robust, and cost-effective means of realizing MCs, which are required by industry.

There are several other features of the proposed MC. It has pure electrostatic optics, which leads to good vacuum conditions suitable for electron guns. It provides a quick response and good reproducibility. Also, this MC has linear optics, which results in easy alignment compared to curved optics. It also offers the high mechanical stiffness of a microscopy column. Furthermore, this MC enables use of the central portion of the beams from the electron source. This differs from a MC with a modified condenser lens, which utilizes the off-axis region of the electron emitter [3]. This improves the stability of the currents and the symmetry of the beam profiles.

In conclusion, we propose a novel monochromator with double cylindrical lenses. They are operated in retarding modes, located in a symmetric condition on the middle plane, and offset to the axis of a microscope. The proposed MC includes two additional round transfer lenses and two apertures. On the mid-plane, energy filtering is realized. The calculated energy dispersion is 23 μm/eV and the estimated energy resolution is better than 10 meV for 4 keV. On the exit plane, stigmatic and lateral dispersion-free imaging of the emitter with unit magnification is achieved. A comparison with other MCs clarifies the pros and cons of the MC. This MC has advantages in its simple structure and high performance. It can bring improvements in the spatial resolutions and energy resolutions of microscopes. In the future, we plan to build the MC and evaluate it in experiments. Further, we will pursue additional improvements by canceling higher aberrations with multipole correctors [15].

References:

[1] H Rose, Ultramicroscopy **78** (1999), p. 13.
[2] HM Mook and P Kruit, Ultramicroscopy **81** (2000), p. 129.
[3] A Henstra *et al*, Microsc. Microanal. **15** (S2) (2009), p. 168.
[4] G Möllenstedt, Optik **5** (1949), p. 499.
[5] H Ohiwa, J. Vac. Sci. Tech. **15** (1978), p. 849.
[6] MR Smith and E Munro, Optik **74** (1986), p. 7.
[7] H Wollnik in "Optics of Charged Particles", (Academic Press, London).
[8] GA Schwind *et al*, J. Vac. Sci. Tech. B **24** (2006), p. 2897.
[9] PC Tiemeijer, Ultramicroscopy **78** (1999), p. 53.
[10] OL Krivanek *et al*, Phil. Trans. R. Soc. A **367** (2009) p. 3683.
[11] M Mukai *et al*, Microsc. Microanal. **12** (S2) (2006) p. 1206CD.
[12] K Tsuno, Nucl. Instr. Meth. A **645** (2011) p. 12.
[13] E Plies *et al*, Nucl. Instr. Meth. A **645** (2011) p. 7.
[14] H Rose and D Krahl in "Energy-Filtering Transmission Electron Microscopy", ed. L Reimer, (Springer-Verlag, Heidelberg), p. 43.
[15] We are very grateful to Prof. T. Ichinokawa from Waseda University for suggesting the energy analyzers with two cylindrical lenses. Grants: 2011-0030233 and 2014R1A6B1A01048695.